Available online at www.sciencedirect.com
SCIENCE DIRECT®
International Journal of Heat and Mass Transfer 48 (2005) 4205–4214
International Journal of HEAT and MASS TRANSFER
www.elsevier.com/locate/ijhmt

Transient performance of an autothermal reformer—A 2-D modeling approach

S.H. Chan *, D.L. Hoang, O.L. Ding

Fuel Cell Strategic Research Programme, School of Mechanical and Production Engineering, Nanyang Technological University, 50 Nanyang Avenue, Singapore 639798, Singapore

Received 17 March 2004; received in revised form 8 December 2004
Available online 17 June 2005

Abstract

The transient performance of an autothermal reformer with methane as the feedstock fuel is studied by modeling approach. The reformer is of cylindrical shape with 60 mm in diameter and 350 mm in length filled with spherical Ni catalyst with 1.75 mm in diameter. A two-dimensional heterogeneous reformer model has been successfully developed to predict the dynamic performance of the reformer subjected to a step-up, a step-down and a sudden change of square-pulse flow rate. The model includes four main simultaneous chemical kinetic reactions involving six species with detailed kinetic conversion and heat and mass transfer phenomena in the reformer. Results showed that there are serious overshoot/undershoot of performance related parameters in the transients, whose values are quite different from those under the steady state conditions.

Keywords: Transient autothermal reforming; Methane reforming; Kinetic modeling

1. Introduction

Global interest in renewable power sources to curb current fuel emission levels makes the development of a new fuel cell system an attractive proposition. Among all fuel cell options, polymer electrolyte membrane fuel cell (PEMFC) is considered to be the most promising technology with immediate/potential market exploitation. However, for this technology to be commercially viable not only its performance needs to be further optimized, it has to be cost competitive with current energy conversion devices. In addition, current PEMFC is relied on hydrogen as the fuel, which underlines the critical issue of fuel supply before its large-scale application. Fuel reforming on methane [1,2], natural gas [3,4], methanol [5,6], fossil fuels [7,8], etc., in particular for fuel cell applications, has been a hot subject for research in recent years. Most studies were focused on the steady-state operation of the reformers, toying with the effect of air–fuel ratio and/or water–fuel ratio on the reformers' performance. Though optimized operating conditions for the reformers can be obtainable from such studies, there are always questions on how the reformer would react/perform under off-design, cold-start or transient operating conditions.

Privette et al. [9] highlighted that one of the two major technical barriers for practical on-board fuel

* Corresponding author. Tel.: +65 6790 4862; fax: +65 6791 1859.
E-mail address: mshchan@ntu.edu.sg (S.H. Chan).

0017-9310/$ - see front matter © 2005 Elsevier Ltd. All rights reserved.
doi:10.1016/j.ijheatmasstransfer.2005.02.042

processing is the rapid start-up/transient response. Wild et al. [10] reported the problems associated with packed bed methanol reformers such as occurrence of cold/hot spots and the slow response at start-up and during transients. The authors proposed the use of metal-supported catalyst in the autothermal reformer for enhanced heat transfer characteristics, thus improving the dynamic response of the reactor. Robbins et al. [11] developed a simplified transient model based on reported detailed surface chemistry mechanisms to investigate the complex interactions between catalytic combustion and methane steam-reforming in a co-flow heat exchanger where surface combustion drives the endothermic steam reforming on opposite sides of separating plates in alternating channel flows. Chan and Wang [12] conducted thermodynamic and kinetic modeling of a 1-D autothermal reformer based on Reitz et al.'s reaction rate of methanol [13]. When operate at 2.7 g/s (air–fuel ratio of 1.19 and water–fuel ratio of 0.5), the cylindrical reformer with a diameter of 60 mm and a length of 200 mm could reach the steady state after 130 s of operation from a step-up temperature change. Beckhaus et al. [14] developed a simulation program with a simple kinetic model to predict the step response of a complete steam reformer system, which includes the heat exchangers and shift reactors. Springmann et al. [15] developed a 1-D, multiphase model to simulate the cold-start behavior of a gasoline based fuel processor and proposed different cold start strategies which includes λ-control, reactive heat up the high-temperature-shift (HTS) reactor by partial oxidation of the reformate with injected air and the use of electrically heated HTS. These techniques are actually adopted from those applied to shorten the cold-start time of automotive 3-way catalytic converters [16,17]. Glöckler et al. [18] analyzed the transient phenomena of a reverse-flow reactor for autothermal methane steam reforming by means of a simplified model. They pointed out that the main shortcoming of this reactor is mainly due to the inefficient heat integration between the periodic processes of endothermic and exothermic reactions leading to poor reactor performance.

Literature review shows that only a handful of studies were focused on the transient operation of a reactor with very limited results showing how the reactor would respond to a critical change in feedstock flow rate, in particular for autothermal reformer. The objective of this study is to investigate the transient performance of an autothermal reformer subjected to different feedstock square-pulse flows. First the optimal air–fuel ratio and water–fuel ratio for the maximum hydrogen yield are determined. Then, the effect of space velocity on the reformed gases is studied so that realistic change in feedstock flow rate is known. Finally, the transient operation of the reformer is conducted based on the optimal/acceptable settings determined above.

2. Kinetic model

2.1. Chemical reaction scheme

To reduce the complexity in the development of a mathematical model for a catalytic reformer with many reactions taking place, only those with significant reaction rate are considered. Based on chemical reactions of partial oxidation [19] and steam reforming of methane [20], it can easily come up with 8 autothermal-related reactions, where the main ones include exothermic complete oxidation, followed by steam reforming, water–gas shift and CO_2 reforming reactions of methane. Other side reactions include cracking of methane and carbon monoxide to carbon deposition, and gasifying carbon by steam and oxygen. However, in these 8 reactions, some reactions actually arrive from the combination of the others, while some have insignificantly low rate of reactions. Thermodynamic analysis showed that optimal H_2 yield (2 moles of H_2 per mole of CH_4 supply) could be expected for a wide range of W/F ratio (1–4) at A/F ratio of 3. Under these A/F and W/F settings for natural gas autothermal reforming, Chan et al. [21] showed that the carbon deposition is not an issue. Thus, all reactions related to carbon deposition and carbon gasification can be ignored provided that the settings of A/F and W/F fall within the above-mentioned range. As a consequence, only the following 4 major reactions are considered:

$$CH_4 + 2O_2 \rightarrow CO_2 + 2H_2O, \quad \Delta H_{1(298)} = -802{,}000\ \text{kJ/kmol} \tag{1}$$

$$CH_4 + H_2O \leftrightarrow CO + 3H_2, \quad \Delta H_{2(298)} = 206{,}000\ \text{kJ/kmol} \tag{2}$$

$$CO + H_2O \leftrightarrow CO_2 + H_2, \quad \Delta H_{3(298)} = -41{,}000\ \text{kJ/kmol} \tag{3}$$

$$CH_4 + 2H_2O \leftrightarrow CO_2 + 4H_2, \quad \Delta H_{4(298)} = 165{,}000\ \text{kJ/kmol} \tag{4}$$

To operate an autothermal reformer, first, the methane and air are fed to the reformer for combustion to heat up the reactor. When the catalyst temperature reaches about 300 °C [22], at which the autothermal reaction can be self activated (or known as lightoff), the preset mixture of methane, air and water is fed to the reformer. In brief, the model considers 4 principal reactions and 6 gas species, i.e., methane (CH_4), oxygen (O_2), carbon dioxide (CO_2), water (H_2O), carbon monoxide (CO) and hydrogen (H_2) in chemical kinetics.

2.2. Reaction rate equations

The rate equation associated with reaction (1) is obtained from Ma et al. [23], while the rate equations for the other 3 reactions are obtained from Xu and Froment [20] as follows:

$$R_1 = \frac{k_1 p_{CH_4} p_{O_2}^{1/2}}{(1 + K^C_{CH_4} p_{CH_4} + K^C_{O_2} p_{O_2}^{1/2})^2} \quad (5)$$

$$R_2 = \frac{k_2}{p_{H_2}^{2.5}} \left(p_{CH_4} p_{H_2O} - \frac{p_{H_2}^3 p_{CO}}{K_{e2}} \right) \times \frac{1}{Q_r^2} \quad (6)$$

$$R_3 = \frac{k_3}{p_{H_2}} \left(p_{CO} p_{H_2O} - \frac{p_{H_2} p_{CO_2}}{K_{e3}} \right) \times \frac{1}{Q_r^2} \quad (7)$$

$$R_4 = \frac{k_4}{p_{H_2}^{3.5}} \left(p_{CH_4} p_{H_2O}^2 - \frac{p_{H_2}^4 p_{CO_2}}{K_{e4}} \right) \times \frac{1}{Q_r^2} \quad (8)$$

$$Q_r = 1 + K_{CO} p_{CO} + K_{H_2} p_{H_2} + K_{CH_4} p_{CH_4} + \frac{K_{H_2O} p_{H_2O}}{p_{H_2}}$$

where R_j (kmol/kgcat h) is the rate of reaction j; $k_j = k_{oj} \times e^{\frac{-E_j}{RT}}$ is kinetic rate constant of reactions j (k_1 is from Ma et al. [23] and k_2, k_3, and k_4 are from Xu and Froment [20]); p_i (bar) is the partial pressure of gas species i. The kinetic data are shown in Table 1. k_{oj} is a constant, E_j (kJ/kmol) is the activation energy, R (kJ/kmol K) is the universal gas constant; T (K) is the gas temperature in the reaction zone; K_{ej} is the equilibrium constant of reaction j (j = 2–4) and can be found in Table 2; $K_i^C = K_{oi}^C \times e^{\frac{-\Delta H_i^C}{RT}}$ is the adsorption constant of species i ($i = CH_4$, O_2) in reaction (1) and can be found in Table 3; $K_i = K_{oi} \times e^{\frac{-\Delta H_i}{RT}}$ is the adsorption constant of species i (i = CO, H_2, CH_4, H_2O) in reactions (2)–(4), which can be found in Table 3.

The rate of consumption or formation of an individual gas species based on reactions (1)–(4) is determined by summing up the reaction rates of that species in all 4 reactions. It should be noted that, when standard industrial catalyst pellet (instead of fine catalyst powder used in the laboratory) is used, one has to consider the intraparticle mass transport limitations [24], which significantly reduce the reaction rates in Eqs. (5)–(8). To account for this shortcoming, average reaction rates were suggested by Groote and Froment [19], which can be determined by multiplying the rate equations (5)–(8) by various effectiveness factors $\eta_1 = 0.05$, $\eta_2 = 0.07$, $\eta_3 = 0.7$, $\eta_4 = 0.06$, respectively. Hence,

$$r_{CH_4} = -\eta_1 R_1 - \eta_2 R_2 - \eta_4 R_4 \quad (9)$$

$$r_{O_2} = -2\eta_1 R_1 \quad (10)$$

$$r_{CO_2} = \eta_1 R_1 + \eta_3 R_3 + \eta_4 R_4 \quad (11)$$

$$r_{H_2O} = 2\eta_1 R_1 - \eta_2 R_2 - \eta_3 R_3 - 2\eta_4 R_4 \quad (12)$$

$$r_{CO} = \eta_2 R_2 - \eta_3 R_3 \quad (13)$$

$$r_{H_2} = 3\eta_2 R_2 + \eta_3 R_3 + 4\eta_4 R_4 \quad (14)$$

where r_i is the conversion rate of gas species i.

Table 1
Kinetic parameters

Reaction	k_{oj} (kmol/kgcat h)	E_j (kJ/kmol)
1	5.852×10^{17} bar$^{-1.5}$	204,000
2	4.225×10^{15} bar$^{0.5}$	240,100
3	1.955×10^{6} bar^{-1}	67,130
4	1.020×10^{15} bar$^{0.5}$	243,900

Table 2
Equilibrium constants

Reaction	Equilibrium constant K_{ej}
2	$5.75 \times 10^{12} \exp(-11{,}476/T)$ (bar^2)
3	$1.26 \times 10^{-2} \exp(4639/T)$
4	$7.24 \times 10^{10} \exp(-21{,}646/T)$ (bar^2)

Table 3
Adsorption constants

Species	K_{oi} (bar^{-1})	ΔH_i (kJ/kmol)
CH_4	4.02×10^5	103,500
O_2	5.08×10^4 bar$^{0.5}$	66,200
CH_4	6.65×10^{-4}	−38,280
CO	8.23×10^{-5}	−70,650
H_2	6.12×10^{-9}	−82,900
H_2O	1.77×10^5 bar	88,680

2.3. Reformer model

Fig. 1 shows the schematic of a 2-D reformer model in (r, z) coordinates. The reformer is of cylindrical shape with 60 mm in diameter and 350 mm in length (i.e. about 0.99 l in volume), filled with spherical Ni catalyst of 1.75 mm in diameter with 9.8% active metal. Since the autothermal reactor normally operates at temperature lower than 1000 °C, the heat radiation can be omitted [25]. The model assumes that the gas flow and properties at the inlet and exit cross-section of the reactor are uniform. The mass and energy balance for the gas phase and solid phase of the reformer are established as follows:

Mass and energy balance equations in the gas phase:

$$\varepsilon \frac{\partial C_i}{\partial t} = D_i \left(\frac{\partial^2 C_i}{\partial r^2} + \frac{1}{r} \frac{\partial C_i}{\partial r} + \frac{\partial^2 C_i}{\partial z^2} \right) - u \frac{\partial C_i}{\partial z} + h_{D_i} S_{cat} (C_{si} - C_i) \quad (15a)$$

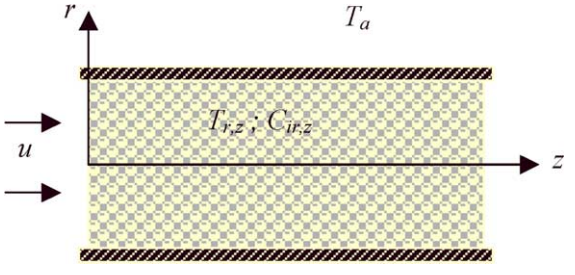

Fig. 1. Schematic of a 2-D reformer thermodynamic model.

$$\varepsilon\rho_g c_{pg}\frac{\partial T_g}{\partial t} = -u\rho_g c_{pg}\frac{\partial T_g}{\partial z} + S_h h(T - T_g) \tag{16}$$

Mass and energy balance equations in the solid phase:

$$\rho_{cat} r_i \frac{M}{\rho_g} = h_{D_i} S_{cat}(C_{si} - C_i) \tag{17}$$

$$\rho_b c_{pb}\frac{\partial T}{\partial t} = K\left(\frac{\partial^2 T}{\partial r^2} + \frac{1}{r}\frac{\partial T}{\partial r} + \frac{\partial^2 T}{\partial z^2}\right) + S_h h(T_g - T) + \rho_{cat}\sum_{j=1}^{4}(-\Delta H_j)\eta_j R_j \tag{18a}$$

where i denotes the gas species; j denotes reaction index; ρ_g, ρ_{cat}, ρ_b (kg/m^3) are the densities of gas, catalyst and bulk catalyst bed, respectively; c_{pg}, c_{pb} (J/kg K) are the specific heats of gas and of catalyst bed, respectively; ε is the void fraction of catalyst bed; M is molecular mass of gas mixture (kg/mol); h_{D_i} (m/s) is the mass transfer coefficient of gas component i; h (W/m^{2}K) is the heat transfer coefficient; T, T_g (K) are the temperature of solid phase and gas phase, respectively; C_{si}, C_i are the mole fractions of gas species i on the catalyst surface and in the gas phase, respectively; r, z (m) are cylindrical coordinates; S_h (m^2/m^3) is the heat transfer area per unit volume of catalyst bed; S_{cat} (m^2/m^3) is the catalyst surface area per unit volume of catalyst bed; ΔH_j (J/mol) is the enthalpy of reaction j; K (W/mK) is the heat conduction coefficient of catalyst bed; u (m/s) is the superficial gas velocity, i.e., the ratio of volume flow rate to the cross section area of the reformer.

Based on the phenomena of the gas flow and operating conditions of the reformer, the initial and boundary conditions are set as follows:

(a) Initial condition $t = 0$: The catalyst is assumed to have reached the lightoff temperature and C_s is either equal to 0 or to the steady-state value of the previous run, i.e.,

$$T = T_0; \quad C_s = C_{s0}; \tag{19}$$

(b) At the reformer inlet face $z = 0$

$$T_g = T_g^{in}; \quad C_i = C_i^{in} \tag{20}$$

(c) At the reformer outlet face $z = L$

$$\frac{\partial C_i}{\partial z} = 0; \quad \frac{\partial T_g}{\partial z} = 0; \tag{21}$$

(d) At the reformer centre $r = 0$

$$\frac{\partial C_i}{\partial r} = 0; \quad \frac{\partial T_g}{\partial r} = 0; \tag{22}$$

With this condition, Eqs. (15a) and (18a) can be replaced by Eqs. (15b) and (18b), respectively

$$\varepsilon\frac{\partial C_i}{\partial t} = D_i\left(2\frac{\partial^2 C_i}{\partial r^2} + \frac{\partial^2 C_i}{\partial z^2}\right) - u\frac{\partial C_i}{\partial z} + h_{D_i} S_{cat}(C_{si} - C_i) \tag{15b}$$

$$\rho_b c_{pb}\frac{\partial T}{\partial t} = K\left(2\frac{\partial^2 T}{\partial r^2} + \frac{\partial^2 T}{\partial z^2}\right) + S_h h(T_g - T) + \rho_{cat}\sum_{j=1}^{4}(-\Delta H_j)\eta_j R_j \tag{18b}$$

(e) At the interfacial surface of inner reformer wall and catalyst bed $r = R$

$$\frac{\partial C_{gi}}{\partial r} = 0; \quad (K + k_g)\frac{\partial T}{\partial r} = \alpha(T - T_a); \tag{23}$$

where T_a is the ambient temperature; α is the overall heat transfer coefficient through the reformer wall; K, k_g (W/mK) are the heat conduction coefficient of the catalyst bed and gas, respectively.

2.4. Gas properties

The gas properties in the reformer, ρ_g and c_{pg}, depend on the temperature and composition of the gas mixture. k_g depends on the temperature and specific heat of the gas [26] and, hence, the composition of the gas mixture. These gas properties vary in the reformer spatially and temporally. They can be determined from the properties and mass fractions of the individual species of the gas mixture. The properties of individual gas are taken from [26,27] as algebraic functions of temperature. Therefore, at each point in the reformer, once the temperature and mole or mass fractions of the gas mixture are known, the bulk gas properties can be determined.

2.5. Heat and mass transfer coefficients

(a) Heat transfer coefficient between catalyst and gas, h (W/m^2 K), is determined using Colburn factor J_H [28] as

$$h = J_H\frac{c_{pg}G_0}{(Pr)^{2/3}} \tag{24}$$

where

$$J_H = 0.91Re^{-0.51}\psi \quad (Re < 50) \tag{25}$$

$$J_H = 0.61Re^{-0.41}\psi \quad (Re > 50) \tag{26}$$

$$Re = \frac{G_0}{S_{geo}\mu_g\psi}$$

Pr is the Prandtl number; ψ is a coefficient depending on the pellet shape ($\psi = 1$ for spherical shape); G_0 (kg/(s m^2)) is the superficial mass flow

rate, defined as mass flow rate $\dot{m}$ divided by the cross section area of the reformer (S), i.e., $G_0 = \frac{\dot{m}}{S}$.

(b) Mass transfer coefficient between catalyst and gas, h_{D_i} (m/s), is determined similar to that of heat transfer by setting $J_D = J_H$ in Eq. (25) [28]

$$h_{D_i} = J_D \frac{G_0}{\rho_g (Sc_i)^{2/3}} \tag{27}$$

$$Sc_i = \frac{\mu_g}{\rho_g D_i} \tag{28}$$

where D_i (m^2/s) is the gas diffusivity of species i, which can be calculated using Slattery–Bird formula [28].

(c) Overall heat transfer coefficient through the reformer wall, α, is determined from

$$\frac{1}{\alpha} = \frac{1}{h_i} + \frac{b}{\lambda} + \frac{1}{h_o} \tag{29}$$

where b is thickness of the reformer wall (m); h_i and h_o are the heat transfer coefficient on the inside and outside of the reformer wall (W/m^{2}K), respectively, while λ is the heat conduction coefficient of the reformer wall (W/mK), which is taken from [29]; h_i is taken from Cussler [30], and h_o is for free convection and is obtained from [31,32].

$$h_i = \frac{0.027 C_c k_g}{d_i} \left(\frac{d_i u_z \rho_g}{\mu_g}\right)^{0.8} \left(\frac{\mu_g c_{pg}}{k_g}\right)^{0.33} \tag{30}$$

$$h_o = \frac{k_a}{d_o} \left(0.6 + \frac{0.387 Ra^{1/6}}{[1 + (0.559/Pr)^{9/16}]^{8/27}}\right)^2 \tag{31}$$

$$Ra = \frac{d_o^3 g \beta (T_{wo} - T_a)}{v_a^2} Pr \tag{32}$$

where Ra is the Rayleigh number; μ_g (kg/ms) is dynamic viscosity of the gas mixture; u_z (m/s) is the gas velocity in z direction; C_c is a constant; d_i, d_o (m) are the inner and outer diameter of the reformer; T_{wo}, T_a (K) are the outer wall and ambient temperatures; g (m/s^2) is the gravitational acceleration; k_a, v_a, β are the heat conduction coefficient, kinetic viscosity and thermal expansion coefficient of the ambient air.

The set of 4 governing equations (15a), (16), (17), (18a) with initial and boundary conditions, Eqs. (19)–(23), in conjunction with the heat and mass transfer coefficients, Eqs. (24)–(32), is then solved for the temperature and gas concentration along and across the reformer using a finite difference method. The overall temperature and compositions of the product gas are derived from the predicted values at different space elements at the rear face of the reformer based on the principle of mixing gas.

3. Results and discussion

With initial and boundary conditions as well as the operating parameters set, the program will run until the convergence criteria are met. All running cases begin with steady state, then follows by transients. Since autothermal reforming process can start only when the light-off temperature is attained, in this study, the initial catalyst bed temperature is set to 700 K (427 °C). In addition, the feed gas temperature and pressure are set to 400 K (127 °C) and 1 atm, respectively. The simulation is carried out with different compositions of methane, air and water. The reformer is essentially a tube reactor made of stainless steel. Without having to consider the insulator material used, the free convective heat transfer coefficient at the outer surface of the stainless steel is scaled down by 5 times to simulate the insulation.

The predicted results of reformer's conversion behavior under different steady state conditions are shown in Figs. 2–9.

Figs. 2 and 3 show the distributions of reformed gas (products) temperature and wet concentrations of H_2, H_2O, CO and CH_4 versus time from the initial state with air-to-fuel ratio (A/F) of 3.5, water-to-fuel ratio (W/F) of 1.5 and space velocity (SV) of 20,000/h. The results

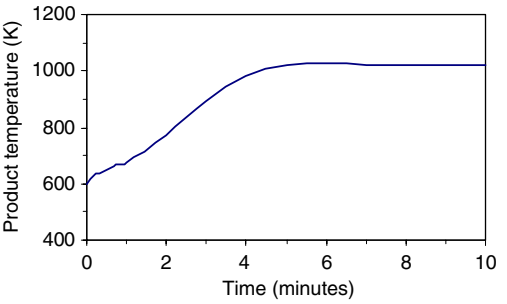

Fig. 2. Reformed gas temperature distribution versus time at A/F = 3.5, W/F = 1.5, SV = 20,000/h.

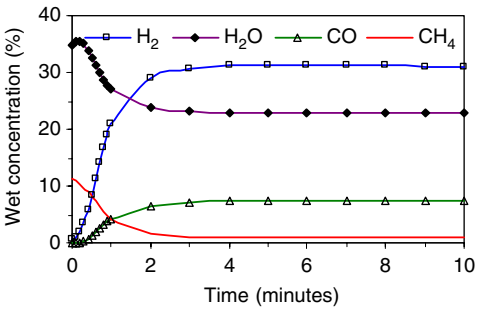

Fig. 3. Wet concentrations of reformed gas versus time at A/F = 3.5, W/F = 1.5, SV = 20,000/h.

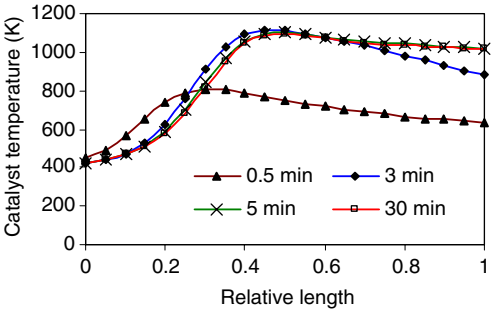

Fig. 4. Catalyst temperature along reformer's length at different time and A/F = 3.5, W/F = 1.5, SV = 20,000/h.

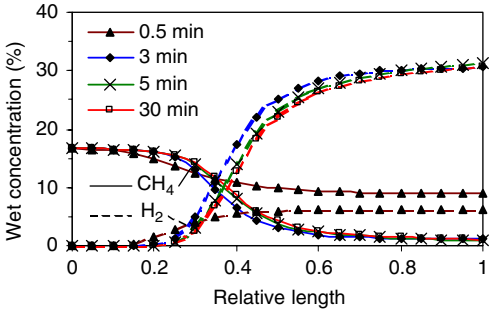

Fig. 5. Wet concentrations of H_2 and CH_4 inside the reformer at A/F = 3.5, W/F = 1.5, SV = 20,000/h.

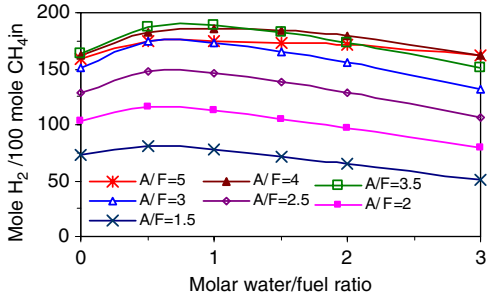

Fig. 6. H_2 yield per 100 moles of CH_4 supplied at different A/F and W/F, SV = 20,000/h.

show that during the first 5 min of the operation, the gas temperature gradually increases with changing of gas concentrations. The reactants such as CH_4 and H_2O decrease while product gases such as H_2 and CO increase. However, after 5 min of operation, the product temperature and concentrations of the reformed gases remain almost unchanged, i.e., the process has reached its steady state. With this feed gas condition, the H_2 yield of about 30%, CO yield of about 6% and the CH_4 residual of about 1% on wet basis have been achieved. The gas temperature is around 1000 K.

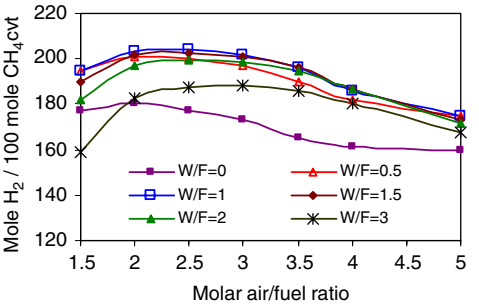

Fig. 7. H_2 yield per 100 moles CH_4 converted at different A/F and W/F, SV = 20,000/h.

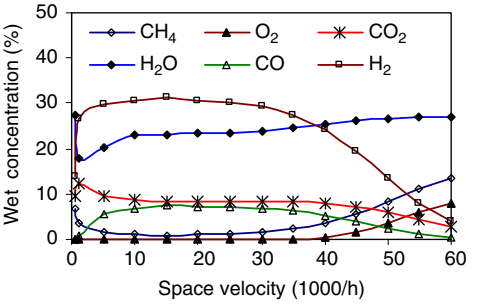

Fig. 8. Wet concentrations of reformed gas vs. space velocity at A/F = 3.5, W/F = 1.5.

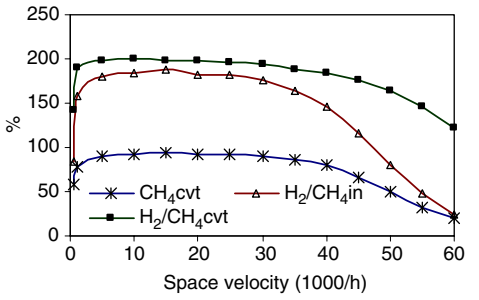

Fig. 9. Conversion efficiency of reformer vs. space velocity at A/F = 3.5, W/F = 1.5.

Figs. 4 and 5 show the distributions of catalyst temperature and H_2 and CH_4 concentrations inside the reformer and along its length at different time marks (0.5, 3, 5, and 30 min) under the same inlet gas conditions as mentioned above. It can be seen that, the temperature curve is changing from time to time in the first 5 min before reaching its steady state. The almost overlapping temperature curves at 5 and 30 min implies that the reformer has more-or-less reached a steady thermal state after 5 min of operation. During the transient

period, the catalyst temperature near the front face decreases with time due to the effect of local heat transfer to the feed gas that is at much lower temperature. In the other part of the reformer, the temperature increases with time until the reformer reaches the fully warmed-up state. The concentration curve at 5 min almost coincides with that at 30 min, showing the same behavior as that of temperature curves. This, again, confirms that the reforming process can reach almost a steady state after 5 min of operation.

Figs. 6 and 7 show the mole number of H_2 produced per 100 moles of CH_4 supplied and per 100 moles of CH_4 consumed, respectively, under different A/F and W/F ratios at space velocity (SV) of 20,000/h. As can be seen from Fig. 6, the highest mole number of H_2 produced per 100 moles of CH_4 supplied is 190 at A/F of 3.5 and W/F of 1. The highest mole number of H_2 produced per 100 moles of CH_4 consumed is about 202 at A/F of 2.5 and W/F of 1 as shown in Fig. 7. However, under this condition, CH_4 conversion is only about 75%, which is much lower than that at A/F of 3.5 and W/F of 1 as mentioned above.

Figs. 8 and 9 show the variations of wet species concentration of reformed gases and conversion efficiency of the reformer as a function of SV of the feed gas with A/F of 3.5 and W/F of 1.5. It can be seen from Fig. 8 that H_2 yield is high in the SV range of 5000/h–35,000/h. Beyond this range, the flow condition is not favorable for conversions. Too low the SV, i.e., too slow feedstock flow, leads to low heat release and thus low reformer temperature which results in low reaction rate and low H_2 yield. Contrarily, too high the SV causes too short the residence time for complete reactions to be carried out, and cool down catalyst in the front part of the reformer because the inlet gas temperature (400 K) is much lower than the catalyst temperature at steady operation (around 1000 K). The consequence is to lower the chemical reaction rate, leading to increased non-reacted fuel. The reformer efficiency can be assessed by judging the CH_4 conversion efficiency (CH_4cvt, i.e., the difference in mole number of CH_4 between the inlet and outlet of the reformer divided by the mole number of CH_4 supplied), the ratio of the mole number of H_2 in the product to 100 moles of CH_4 supplied, or the ratio of the mole number of H_2 in the product to the mole number of CH_4 converted (consumed). The variations of conversion efficiencies are presented in Fig. 9. Similar to the concentration curves, it can be seen that the efficiencies are high within the SV range of 5000/h–35,000/h. CH_4 conversion efficiency reaches 98% with 185 moles of H_2 produced per 100 moles of CH_4 supplied. For 100 moles of CH_4 consumed, 198 moles of H_2 can be produced. Beyond this SV range, the efficiency is poor.

Based on the above study, it is reasonable to set the A/F and W/F to 3 and 1, respectively, and the feed flow rate varying in the range of 7000–28,000 l/h for the transient study. There are three transient cases under investigation:

Case A. A big square-pulse transient flow rate with pulse width of 20 min to show the effects of step-up and step-down flow rate.

Case B. Two up pulses, one small pulse with pulse width of 2 min and one big pulse with pulse width of 5 min; both have the same pulse height and a long dwell time of 15 min to isolate the interactions between the two pulses.

Case C. Two up pulses each has a pulse width of 5 min separated by a short dwell time of 2 min. The pulse height of the second pulse is twice the value of the first pulse.

Though extensive simulation results are available, only the product gas temperature, H_2 and CO concentrations, CH_4 conversion efficiency and H_2 yield (mole number of H_2 produced per 100 moles of CH_4 supplied) are discussed. To be more focusing on the overshoot/undershoot of the above parameters during transients; the following study puts emphasis on the temporal variation of these parameters at the exit of the reformer.

Fig. 10 shows the results of Case A study. The product temperature at the exit of the reformer overshoots by 26 °C registered at 1039 K (1013 K under steady state), H_2 concentration overshoots by 8.64 vol.% registered at 37.98 vol.% (28.34 vol.% under steady state), CO overshoots by 2.83 vol.% registered at 9.62 vol.% (6.79 vol.% under steady state), CH_4 conversion efficiency overshoots by 14.35% registered at 89.67% (75.32% under steady state) and H_2 yield overshoots by 43.18 moles registered at 184.89 moles (141.66 moles under steady state) when the flow rate is doubled from its initial value of 14,000 l/h. However, when the flow rate is halved from its original flow rate of 28,000 l/h, the product temperature at the exit of the reformer undershoots by 59 °C registered at 843 K (902 K under steady state), H_2 concentration undershoots by 12.44 vol.% registered at 18.75 vol.% (31.19 vol.% under steady state), CO undershoots by 3.76 vol.% registered at 3.82 vol.% (7.58 vol.% under steady state), CH_4 conversion efficiency overshoots by 20.35% registered at 59.64% (79.99% under steady state) and H_2 yield undershoots by 62.20 moles registered at 93.77 moles (155.97 moles under steady state). This case of study indicates a number of interesting phenomena: (1) undershoot is more severe than overshoot during transients, (2) step increase in flow rate causes CO overshoot that would bear a burden on the subsequent CO cleanup, and (3) step decrease in flow rate causes unacceptably low CH_4 conversion.

Fig. 11 shows the results of Case B study. When subject to a square-pulse change in flow rate from 7000 to 28,000 l/h and back to 7000 l/h, the undershoots

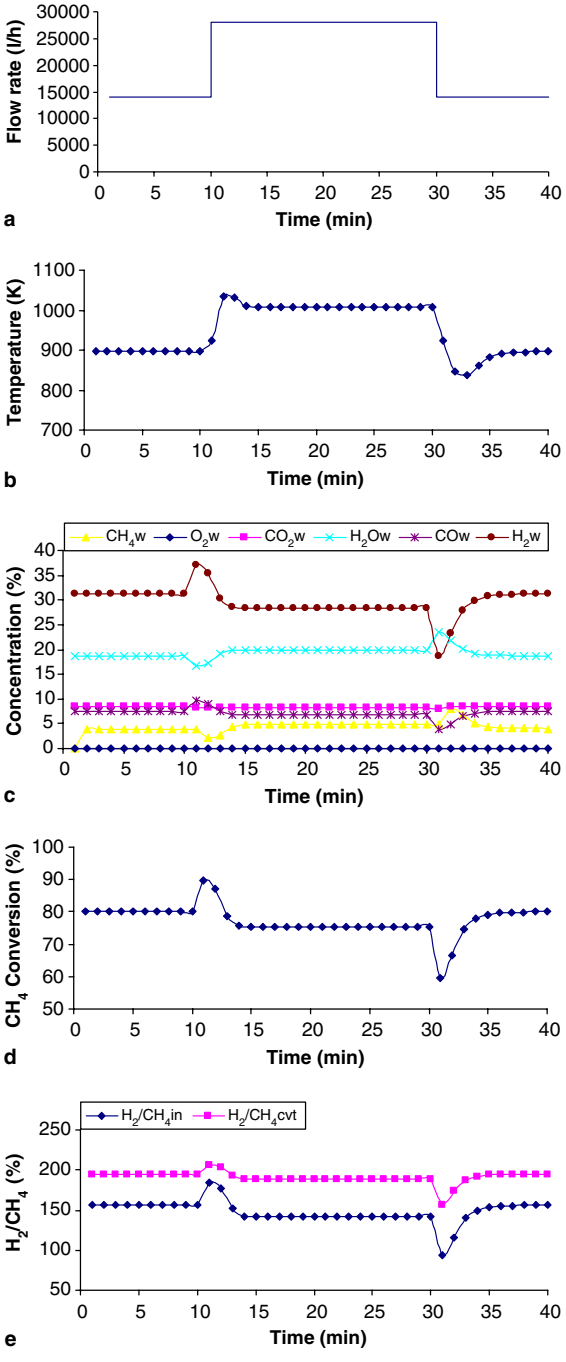

Fig. 10. Transient performance of the reformer (Case A).

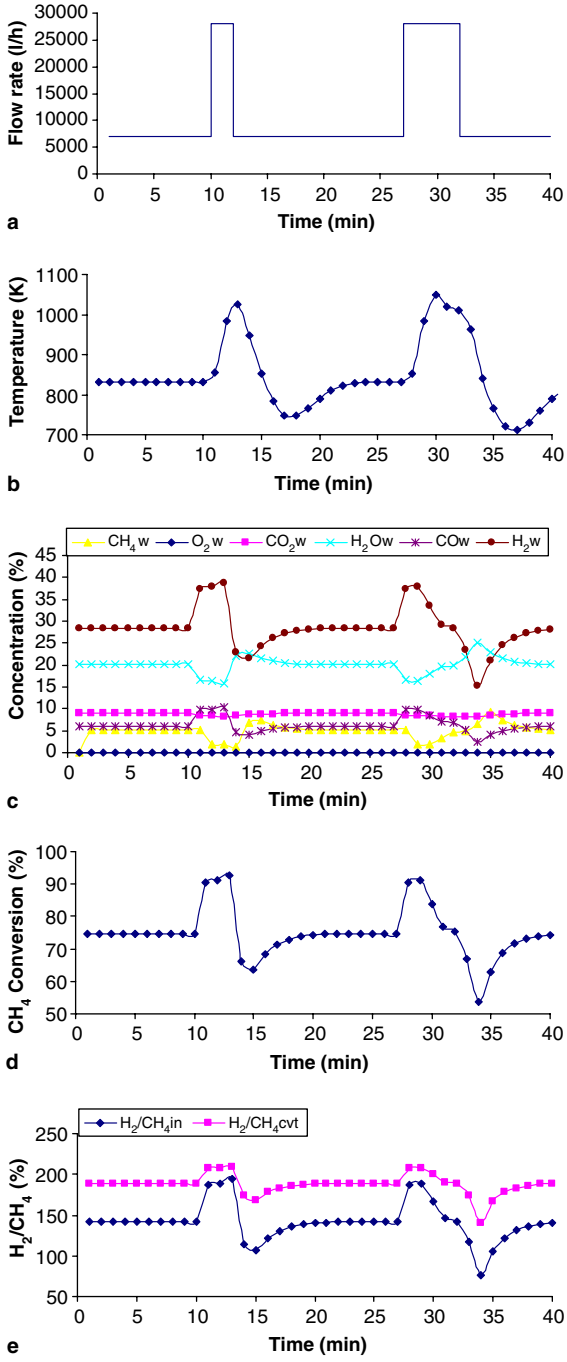

Fig. 11. Transient performance of the reformer (Case B).

(negative peaks) associated with larger pulse width (5 min) are much more severe than those with small pulse width (2 min), i.e., gas temperature: 750 K, H_2: 21.48 vol.%, CO: 4.04 vol.%, CH_4 conversion: 63.64%, H_2 yield: 107.42 moles for smaller pulse width as against gas temperature: 714 K, H_2: 15.16 vol.%, CO: 2.48 vol.%, CH_4 conversion: 53.69%, H_2 yield: 75.81 moles for larger pulse width. As for the overshoots (positive peaks), except the gas temperature, all other parameters show higher overshoot values in the case of smaller pulse width, i.e., gas temperature: 1030 K, H_2: 38.77 vol.%, CO: 10.25 vol.%, CH_4 conversion: 92.77%, H_2 yield:

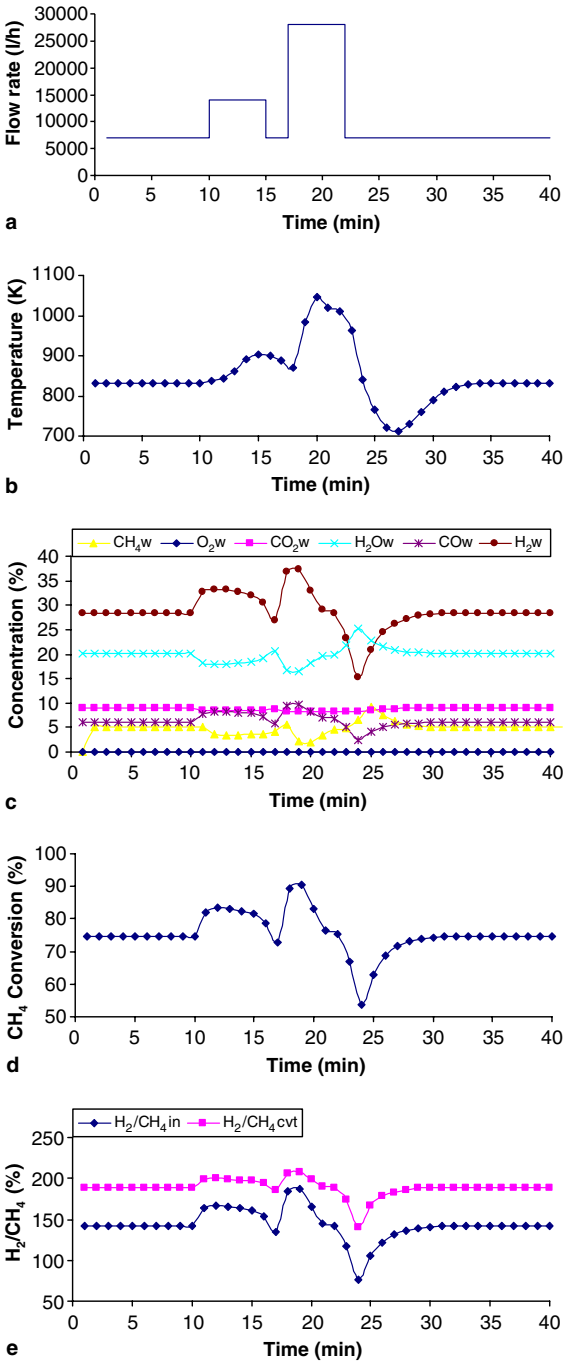

Fig. 12. Transient performance of the reformer (Case C).

193.83 moles for smaller pulse width as against gas temperature: 1057 K, H_2: 37.85 vol.%, CO: 9.90 vol.%, CH_4 conversion: 91.11%, H_2 yield: 189.23 moles for larger pulse width.

Fig. 12 shows the results of Case C study. It is noted that 2 min of dwell time is sufficient to resolve the two pulses clearly. There are very slight undershoots of performance parameters in the first pulse as before they could drop further they have already been picked up by the second pulse effect. Results clearly indicate that the higher the pulse height, the more overshoot/undershoot one would encounter.

Based on the above three cases of study, we could summarize that the overshoot/undershoot of the performance parameters at any point of time during transients are closely related to the temperature and, may be, the water concentration (Figs. 10(c), 11(c) and 12(c)) as the latter has high specific heat that would affect the "stored energy" of the reactor and thus the gas temperature for reactions. Though it is interesting to note that there is momentarily increase in H_2 and CH_4 conversion during transients, the cost is high CO concentration during transients and low H_2 and CH_4 conversion at the end of the transient pulse.

4. Conclusions

A 2-D unsteady model has been successfully developed to predict the transient performance of a cylindrical reformer (60 mm in diameter and 350 mm in length). The simulation was conducted under constant flow temperature and pressure of 400 K and 1 atm, respectively, and initial catalyst temperature of 700 K. Under such conditions, the air–fuel ratio, water–fuel ratio and flow rate of 3, 1 and 7000–28,000 l/h would give the optimal H_2 yield. Thus, all transient cases with square-pulse feedstock flow rate were run under such settings. Results showed that undershoot is more severe than overshoot during transients, step increase in flow rate would cause CO overshoot which pose a burden on the subsequent CO cleanup and step decrease in flow rate would cause unacceptably low CH_4 conversion. In addition, the overshoot/undershoot of the performance parameters during transients are closely related to the temperature and, may be, the water concentration as the latter has high specific heat that would affect gas temperature for reactions. It is interesting to note that there is momentarily increase in H_2 and CH_4 conversion during transients, however, it is at the expense of high CO concentration during transients and low H_2 and CH_4 conversion at the end of the transient pulse.

References

[1] Y.-S. Sea, A. Shirley, S.T. Kolaczkowski, J. Power Sources 108 (2002) 213.
[2] Y. Matsumura, T. Nakamori, Appl. Catal. A: Gen. 258 (2004) 107.
[3] S.H. Chan, H.M. Wang, Fuel Process Technol. 64 (2000) 221.

[4] Z. Chen, P. Pradeep, Y. Yan, S. Elnashaie, Fuel Process Technol. 83 (2003) 235.
[5] S.H. Chan, H.M. Wang, Fuel Int. 1 (1–1) (2000) 17.
[6] S. Liu, K. Takahashi, M. Ayabe, Catal. Today 87 (2003) 247.
[7] C. Pereira, J-M. Bae, S. Ahmad, M. Krumpelt, in: Proc. of the 2000 Hydrogen Program Technical Review, NREL/CP-70-28890, San Ramon, CA, USA.
[8] Q. Ming, T. Healey, L. Allen, P. Irving, Catal. Today 77 (2002) 51.
[9] R.M. Privette, T.J. Flynn, M.A. Perna, K.E. Kneidel, 1999 DOE/EPRI/GRI Fuel Cell Technology Review Conference, 3–5 August 1999, Chicago, IL, USA.
[10] P.J. de Wild, M.J.F.M. Verhaak, Catal. Today 60 (2000) 3.
[11] F.A. Robbins, H. Zhu, G.S. Jackson, Catal. Today 83 (2003) 141.
[12] S.H. Chan, H.M. Wang, J. Power Sources 126 (2004) 8.
[13] T.L. Reitz, S. Ahmad, M. Krumpelt, R. Kumar, H.H. Kung, J. Mol. Catal. A: Chem. 162 (2000) 275.
[14] P. Beckhaus, A. Heinzel, J. Mathiak, J. Roes, J. Power Sources 127 (2004) 294.
[15] S. Springmann, M. Bohnet, A. Docter, A. Lamm, G. Eigenberger, J. Power Sources 128 (2004) 13.
[16] K. Kollman, J. Abthoff, W. Zahn, H. Bischof, J. Gohre, SAE 940472, 1994.
[17] K.H. Hellman, R.I. Bruetsch, G.K. Piotrowski, W.D. Tallent, SAE 890799, 1989.
[18] B. Glöckler, G. Kolios, G. Eigenberger, Chem. Eng. Sci. 58 (2003) 593.
[19] Ann M. De Goote, G.F. Froment, Appl. Catal. A 138 (1996) 245.
[20] J. Xu, G.F. Froment, AIChE J. 35 (1989) 88.
[21] S.H. Chan, O.L. Ding, D.L. Hoang, Int. J. Green Energy 1 (2004) 265.
[22] L. Ma, D.L. Trimm, Appl. Catal. A 138 (1996) 265.
[23] L. Ma, D.L. Trimm, C. Jiang, Appl. Catal. A 138 (1996) 275.
[24] J. Xu, G.F. Froment, AIChE J. 35 (1989) 97.
[25] D. Wolf, M. Hohenberger, M. Baerns, Ind. Eng. Chem. Res. 36 (1997) 3345.
[26] M. Kaviany, Principles of Heat Transfer, Wiley & Sons, New York, 2002.
[27] M.J. Moran, H.N. Shapiro, Fundamentals of Engineering Thermodynamics, John Wiley & Sons, New York, 1992.
[28] R. Byron Bird, W.E. Stewart, E.N. Lightfoot, Transport Phenomena, John Wiley & Sons, New York, 1960.
[29] A.J. Chapman, Heat Transfer, Macmillan Publishing Company, New York, 1984.
[30] E.L. Cussler, Diffusion, Mass Transfer in Fluid Systems, Cambridge University Press, Cambridge, New York, 1984.
[31] S.W. Churchill, H.H.S. Chu, Int. J. Heat Mass Transfer 18 (1975) 1049.
[32] S.H. Chan, D.L. Hoang, Int. J. Heat Mass Transfer 42/22 (1999) 4165.